Journal of CO2 Utilization 70 (2023) 102447

Contents lists available at ScienceDirect

Journal of CO2 Utilization

journal homepage: www.elsevier.com/locate/jcou

AC-driven atmospheric pressure glow discharge co-improves conversion and energy efficiency of CO_2 splitting

Guodong Meng [a,*], Linghan Xia [a], Yonghong Cheng [a], Zongyou Yin [b,*]

[a] State Key Laboratory of Electrical Insulation and Power Equipment, Xi'an Jiaotong University, Xi'an 710049, China
[b] Research School of Chemistry, Australian National University, Canberra, ACT 2601, Australia

ARTICLE INFO

Keywords:
Atmospheric pressure glow discharge
Plasma
AC driving
CO_2 splitting
Electron collision reaction

ABSTRACT

Gap distance and discharge power have great influence on the morphology and characteristics of glow plasma. Unfortunately, there is few research on the influence law and mechanism of these factors for CO_2 splitting by glow plasma. In this study, an AC-driven atmospheric pressure glow discharge (APGD) plasma reactor was developed for CO_2 splitting. Through the rational design on the plasma reactor accompanied by numerical simulation and systematic experimentation, the unique influence laws and mechanisms on CO_2 splitting behavior are unveiled. Several key parameters, such as gap distance, discharge power and gas flow rate, are found able to play synergistic roles in tailoring plasma reactor to co-improve the conversion and energy efficiency. At an optimized gap distance, sufficient electron collisions along the main channel results in the largest active plasma volume, leading to the optimal CO_2 splitting performance. The conversion and energy efficiency could also be co-improved by synchronously increasing the discharge power and gas flow rate at a given specific energy input (SEI) value, which exhibits an opposite feature of dielectric barrier discharge (DBD) plasma, because larger plasma volume increases the probability of collision dissociation reaction and lower gas temperature decreases the rate of recombination reaction. The AC-driven APGD reactor can achieve maximum conversion of 11.96% and maximum energy efficiency of 41.51% which superior to the results of most atmospheric pressure plasmas. This work gains insights into the behaviors of AC-driven APGD plasma in CO_2 splitting and potentially opens an avenue to develop plasma technology for sustainable CO_2 utilization.

1. Introduction

Carbon dioxide (CO_2), as the dominated greenhouse gas, has been continuing to be excessively emitted to the atmospheric environment in the last sixty years, causing a severe global climate problem [1]. While the world takes serious attention on the CO_2 emissions reduction in pursuit of carbon neutrality, various techniques have been proposed to realize the CO_2 storage and conversion [2]. Compared with the high cost of CO_2 storage, converting CO_2 into chemicals with high value-added through catalytic reaction is more favorable. Non thermal plasma (NTP)-catalytic CO_2 decomposition has been emerged as a promising method for CO_2 conversion since it could significantly reduce the reaction temperature and then enable the activation of stable CO_2 molecules under relatively mild conditions [3]. As the gas temperature in NTP is much lower than the electron temperature, electrons with high energy could activate CO_2 molecules to produce new active intermediate products without heating the whole gas [4,5]. Therefore, it is gradually recognized that NTP provides an energy-saving method for CO_2 splitting [6]. From the perspective of industrial application and environmental protection, using photovoltaic and/or wind renewable energy to generate discharge plasma and convert CO_2 into value-added chemicals can effectively solve the problems of both energy utilization and carbon emission.

In general, different types of NTPs are used in CO_2 splitting. Dielectric barrier discharge (DBD) is with a simple structure and suitable for coordination with catalysts [7,8], however, the dissociation of CO_2 basically comes from the direct excitation of CO_2 molecules rather than the vibrational excitation of CO_2 molecules, resulting in a low energy efficiency [9]. Using gliding arc (GA) plasma for CO_2 splitting has a high energy efficiency due to the high proportion of vibrational excitation within the plasma region. Unfortunately, the conversion is still relatively low ($< 8\%$) up to now, because of the poor diffusivity of arc plasma and high gas velocity [10]. Microwave (MW) plasma is also widely used in CO_2 splitting which can make high conversion and energy efficiency

* Corresponding authors.
E-mail addresses: gdmengxjtu@xjtu.edu.cn (G. Meng), zongyou.yin@anu.edu.au (Z. Yin).

https://doi.org/10.1016/j.jcou.2023.102447
Received 3 December 2022; Received in revised form 21 February 2023; Accepted 22 February 2023
Available online 24 February 2023

[11,12], but the atmospheric pressure in the reaction chamber needs to be confined to be below 400 mbar [13], which greatly limits the application scope. Atmospheric Pressure Glow Discharge (APGD) plasma is far from the thermal equilibrium, and the gas temperature (less than 2600 K) is significantly lower than vibration temperature (about 5000 K), which illustrates that APGD is a typical NTP [16]. Lower gas temperature is conducive to reducing vibration translational relaxation, and then benefits increasing energy efficiency in CO_2 splitting [9]. APGD operates stably under low current, and its discharge volume is relatively small, so its power density is high (about 5 $\times 10^7$ W/m^3) [14].

At present, large-scale APGD has been realized through pin-plate electrode [15]. It is of great significance to study the conversion effect and influencing factors of APGD on CO_2. Trenchev et al. [16] used DC-driven APGD for CO_2 splitting, and optimized the APGD reactor by adding vortex nozzles and limiting discharge areas. Under DC driving, the gas temperature in the APGD reactor is high, so it is necessary to use a higher gas flow to reduce the gas temperature and reduce the influence of thermal instability factors in order to achieve stable glow discharge. The increase of gas flow reduces the residence time of CO_2 molecules in the plasma region, which limits the conversion. On the other hand, Tochikubo [17] found that it is easier to obtain stable APGD in high frequency (> 1 kHz) electric field, and using AC high voltage to drive APGD can effectively reduce the influence of thermal instability factors and improve the stability of APGD [18]. Raja et al. [19] studied the influence of gas input mode on CO_2 splitting and achieved competitive energy efficiency but low conversion rate at high gas flow rate. In APGD, gap distance and discharge power have a great influence on the morphology and characteristics of glow plasma [20]. Unfortunately, there is few research on the influence law and mechanism of gap distance and discharge power for CO_2 splitting by APGD at present. Although specific energy input (SEI) is a crucial factor for CO_2 splitting, it is reported that a certain SEI value obtained by different combinations of gas flow rate and discharge power may result in different conversion performances in plasma system [21]. However, the conversion performances of those different combinations in APGD is not clear so far. Therefore, to explore the influences of gap distance, discharge power and gas flow and their synergy on CO_2 splitting by AC-driven APGD is urgently significant under the current global environment where the carbon neutral economy is pursued.

In this work, we have developed a custom-designed AC-driven APGD reactor, and discussed the influence mechanisms of gap distance, discharge power and gas flow on CO_2 splitting through the combination of experiment and finite element model (FEM) simulation. By comparing the influences of different factors systematically, we have explored the synergistic effect of discharge power and gas flow on CO_2 splitting. The corresponding relationship between macroscopic parameters and microscopic physicochemical processes is established through FEM simulation.

2. Experimental setup and simulation

2.1. Experimental setup

Fig. 1(a) shows the schematic diagram of the CO_2 splitting and analysis system. AC high voltage power supply (CTP-200k) is used as glow discharge plasma generator, which can output a maximum voltage of 30 kV with the center frequency of 20 kHz. The ballast resistance is chosen to be 500 kΩ to ensure a stable glow discharge at atmospheric pressure. The discharge voltage is measured by Tektronix high voltage probe (P6015A), while the discharge current is measured by the 50 Ω non-inductive sampling resistance. The discharge voltage and current are monitored through a Tektronix DPO 4032 oscilloscope. The CO_2 gas with purity of 99.99% is feed into the reactor through the gas flow meter (0–1000 mL/min, LZB-3wb) and the gas cylinder. The composition and concentration of the product gas are detected online by gas chromatograph (GC, Bruker scion 456-GC) equipped with a thermal conductivity detector (TCD), and product gases are separated by chromatographic column TDX-01. The mechanical pump is connected in parallel with the GC and connected to the gas product outlet of the reactor. At the beginning of the experiment, the air in the reactor is pumped out by mechanical pump and then CO_2 is introduced, which can ensure the maximum purity of CO_2 in the reactor in a short time.

Specifically, Fig. 1(b) and (c) show the schematic diagram and real picture of the APGD CO_2 splitting reactor. In the reactor, the high voltage electrode is a stainless-steel ring with an inner diameter of 3 mm and an outer diameter of 20 mm. The grounding electrode is a stainless-steel needle with a tip diameter of 1 mm and a length of 80 mm. The outer wall of the reactor is a 2 mm-thick quartz glass tube with an inner diameter of 20 mm. The distance between the pin and the ring electrodes could be adjusted in the range of 1–30 mm. CO_2 gas flow is feed into the reactor from the needle electrode side and the products are carried into the GC for in-situ analysis.

The conversion and energy efficiency are key parameters to characterize the effect of plasma for CO_2 conversion [16]. CO_2 conversion is calculated by the following equation:

$$X_{CO_2}\left[\%\right] = \frac{c_{CO(out)}}{c_{CO(out)} + c_{CO_2(out)}} \times 100\% \quad (1)$$

where, $c_{CO(out)}$ and $c_{CO2(out)}$ are the concentrations of CO and CO_2 out of the reactor, respectively.The energy efficiency is calculated by the following equation:

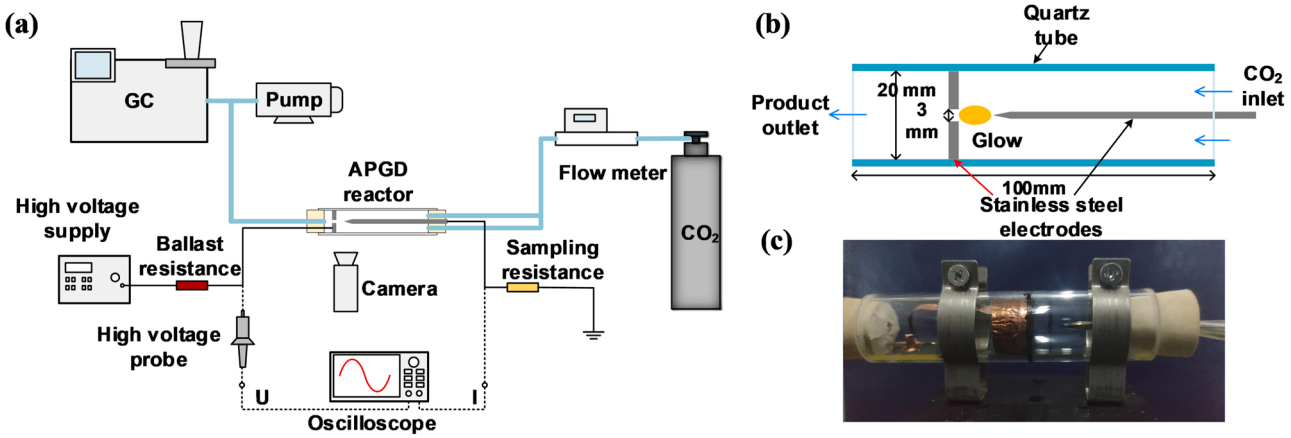

Fig. 1. (a) Schematic diagram of the CO_2 splitting and analysis system, (b) the schematic diagram and (c) real picture of the APGD reactor.

$$\eta\left[\%\right] = \frac{\Delta H_R\left[kJmol^{-1}\right] \times X_{CO_2}\left[\%\right]}{SEI\left[kJL^{-1}\right] \times 22.4Lmol^{-1}} \quad (2)$$

where, ΔH_R is the reaction enthalpy of CO_2 splitting under standard conditions (279.8 kJ mol^{-1}), and *SEI* is the specific energy input. *SEI* is the main parameter determining CO_2 conversion and energy efficiency, which is calculated by the following equation:

$$SEI\left[kJL^{-1}\right] = \frac{\text{Dischargepower}[W]}{\text{Gasflowrate}\left[\frac{mL}{\text{min}}\right]} \times 60\frac{\text{s}}{\text{min}} \quad (3)$$

where, the gas flow rate is defined as standard mL/min (mL/ min), and the discharge power (*P*) is is as follows:

$$P = fW = f\int_{t_0}^{t_0+T} u(t)i(t)dt \quad (4)$$

where, *u(t)* is the discharge voltage, *i(t)* is the current flowing through the reactor, $u_c(t)$ is the voltage across external capacitor, *T* is the discharge cycle, *f* is the discharge frequency of the applied voltage.

2.2. Simulation model and parameters setting

In order to explore the mechanism of AC-driven APGD for CO_2 splitting influenced by gap distance, discharge power and gas flow rate, we built a simulation model based on plasma module and fluid module in COMSOL Multiphysics. In the simulation model, the gas gap distance is set to 4, 6, 8 mm, the voltage amplitude of AC is set to10, 15, 20 kV, the frequency is 22 kHz, and the gas flow rate is set to 250, 300, 350, 400, 450, 500 mL/min. All species considered in the model are shown in Table 1. In the CO_2 plasma simulation model, four neutral species and five charged species, as well as five vibrational excited states and two electronic excited states of CO_2 molecules are considered. CO_2va represents the first bending mode (010), CO_2vb represents the first symmetric stretching mode (100) and the second bending mode (020), CO_2vc represents the first asymmetric stretching mode (001), CO_2vd represents the higher-order symmetric stretching mode (n00) and bending mode (0n0) [22]. CO_2s represents the electronic excited state $1\Sigma_u^+$. The plasma chemical reactions and their reaction coefficients involved in this model are shown in the Supporting Information.

3. Results and discussions

3.1. Discharge plasma characteristics

Fig. 2 shows the typical voltage and current waveforms of APGD at different discharge powers (7.46, 15.24, 20.94 and 23.13 W), in which the gas flow rate is 250 mL/min and gap distance is 6 mm. It's worth noted that the discharge power is changed by adjusting the applied voltage, so the corresponding voltages are 7.9, 11.8, 17.4 and 20.0 kV respectively. It can be seen that the pulse electrical signals appear within the discharge initial period (as shown in Fig. 2(a) and (b)), where the phase of current pulse lags behind the voltage pulse. This is considered as the characteristic of streamer discharge, indicating that streamer discharge occurs before the glow discharge at lower discharge power [23]. That is attributed to the intensification of the electric field at the electron avalanche heads. During the discharge initial period, the space electric field intensity of the electron avalanche heads would become higher than the applied electric field when the applied voltage is low, leading to weakening of electric field in the middle of electron avalanche [18]. The recombination process of positive and negative charges emits photons, causing photoionization and secondary electron avalanche, forming streamer discharge under the distorted electric field of the electron avalanche head. Due to the existence of current limiting resistance, the streamer could not further develop into electric arc, and then form glow discharge. In Fig. 2(c) and (d), it is found that the proportion of pulse signals decrease along with the increase of the applied voltages, since the applied electric field are higher than space electric field of the electron avalanche before breakdown and streamer discharge is difficult to form.The influence of the streamer discharge on CO_2 splitting will be discussed in Section 3.3. Furthermore, it is noteworthy that the discharge voltage decreases with the increase of discharge current, illustrating that the glow discharge is at γ-mode, that is, normal glow discharge [15].

Table 1
All species considered in the model.

Specie types	Species
Atom	O
Molecule	CO_2, CO, O_2
Charged specie	CO_2^+, e, O^-, O^+, O_2^+, O_2^-
Vibrational excited specie	CO_2v1, CO_2va, CO_2vb, CO_2vc, CO_2vd
Electronic excited specie	CO_2s

3.2. The influence of gap distance

Fig. 3(a) shows the CO_2 conversion and energy efficiency as a function of gap distance, in which the gas flow rate is 250 mL/min. Fig. S1 shows the discharge voltage and current waveforms of APGD at different gap distances when the discharge power is kept to approximately 24 W. Since the discharge power and gas flow rate nearly remain unchanged, the SEI value would be a constant, the trends of CO_2 conversion and energy efficiency are similar. The conversion and energy efficiency rise first and then fall with the increase of gap distance. It can be seen that the conversion and energy efficiency curves demonstrate a peak value of 11.80% and 26.54%, respectively, when the gap distance is 6 mm. The conversion is determined by the proportion of CO_2 molecules passing through the plasma region which is related to plasma region volume in this reactor [16]. Fig. 3(b) shows the images of CO_2 glow discharge plasma morphology across different gap distances. The exposure time of these photographs is set to 1/1600 s. The dash red line represents the contour of pin and plate electrodes. In addition to the gap distance, the morphology of the discharge plasma is also related to the discharge current [15]. The mean discharge voltage and current at different gap distances are shown in Fig. 3(c). Since the gap distance increases, the discharge voltage would increase accordingly [24], so the discharge current would decrease in order to keep the same discharge power. The amplitude of discharge current is in a good agreement with luminescent intensity of the plasma channels, as shown in Fig. 3(b). Moreover, it can be also observed that as the gap distance is enlarged, the discharge plasma morphology would vary from a narrow straight channel into a broader obconic shape, and that looks more obvious when the gap distance is larger than 3 mm. The increase in the overall volume of discharge plasma can be explained that, due to the presence of the radial electrical field component inside the gap, lots of charged particles would drift in the radial direction and bring out collision ionization around the main channel, which turn into an obconic shape and equivalently enlarge the plasma volume. As the gap distance increases, the extensions in the radial direction as well as the discharge plasma volume become larger [25], which benefits the CO_2 splitting. However, the discharge current decreases along with the increase of gap distance, which plays a negative role on the CO_2 splitting. Consequently, the conflicting effect between the plasma volume and discharge current reaches an optimum value of CO_2 conversion and energy efficiency while the gap distance is 6 mm, as shown in Fig. 3(a). In summary, with a given discharge power, we could optimize the reactor to achieve co-improved conversion and energy efficiency by setting appropriate gap distance for APGD.

Furthermore, we simulated and plotted the distribution of electron density along the discharge channel as shown in Fig. 4. Fig. 4(a) and (b) show the electron density distribution in positive half circle and negative half circle. CO_2 splitting under APGD conditions is dominated by

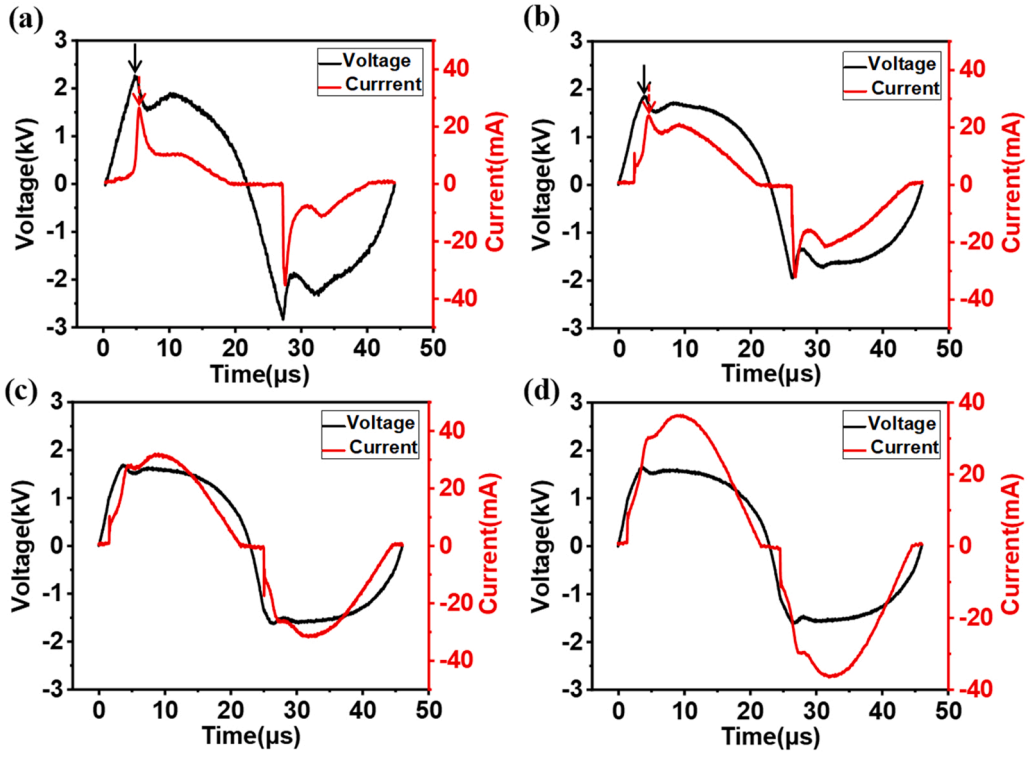

Fig. 2. Voltage and current waveforms of APGD at different discharge powers: (a) 7.46 W, (b) 15.24 W, (c) 20.94 W and (d) 23.13 W.

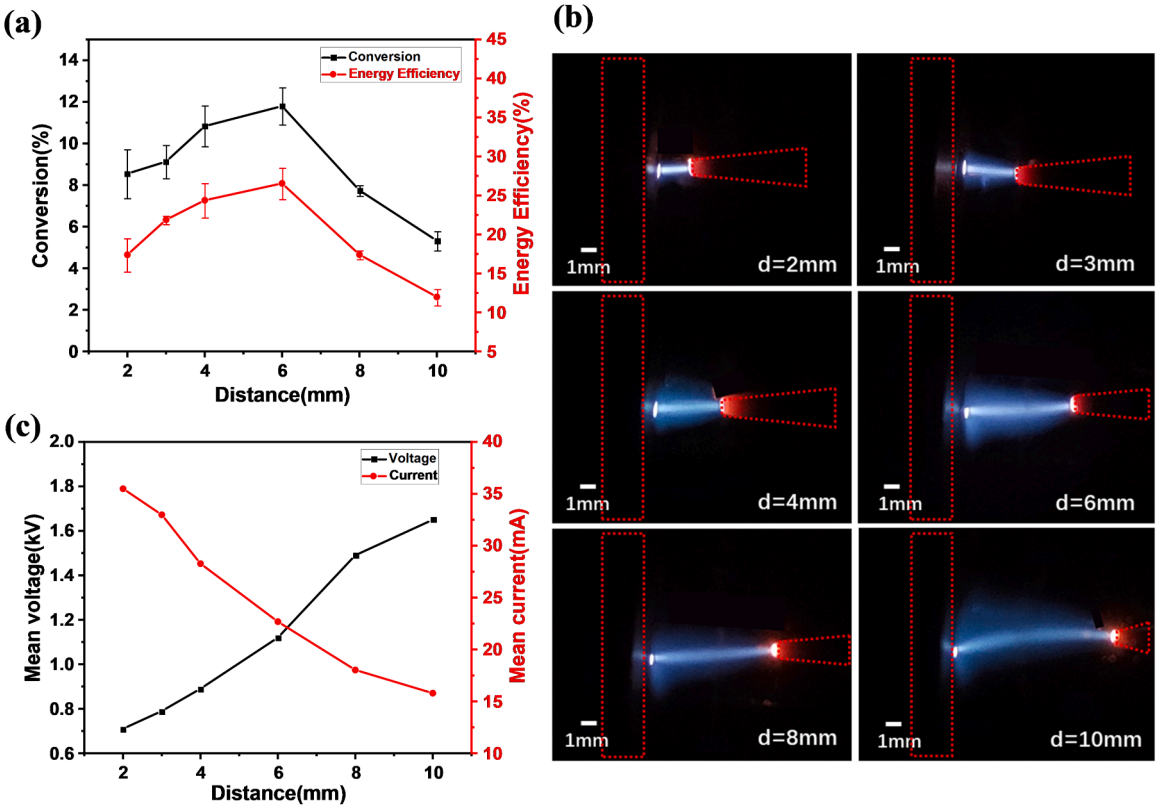

Fig. 3. (a) CO_2 conversion and energy efficiency as a function of gap distance, (b) images of CO_2 glow discharge plasma and (c) mean voltage and current at different gap distances.

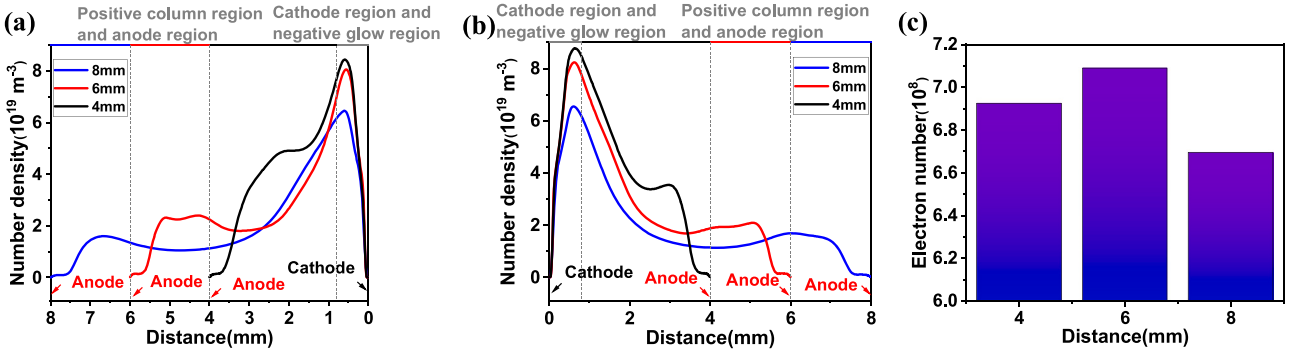

Fig. 4. Simulation results of electron density distribution along discharge channel: (a) positive half circle, (b) negative half circle and (c) the total electron number in a complete discharge circle.

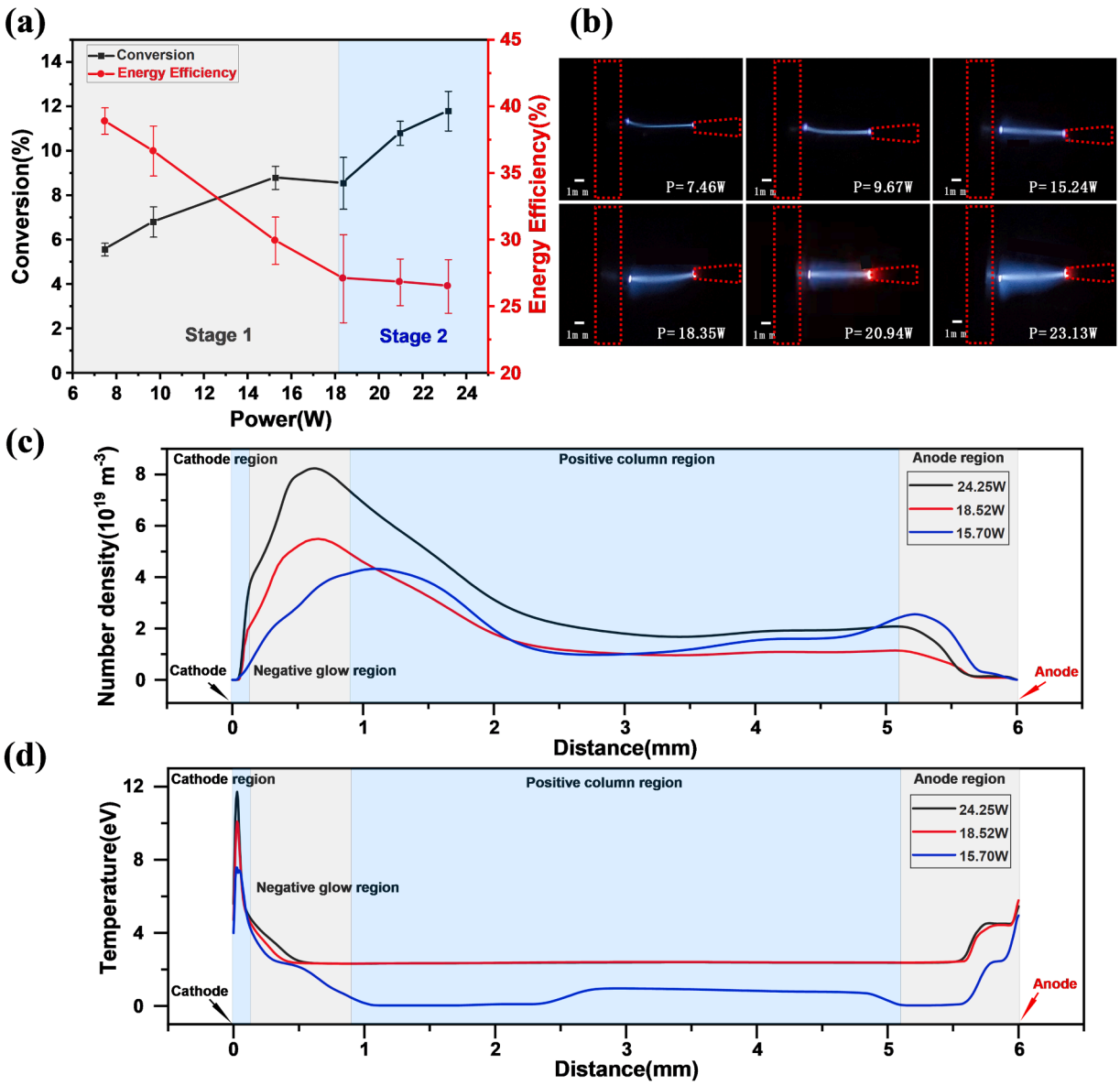

Fig. 5. (a) CO_2 conversion and energy efficiency as a function of discharge power, (b) the images of CO_2 glow discharge at different discharge powers, (c) simulation results of electron density distribution along discharge channel in the negative half cycle, and (b) simulation results of electron temperature distribution along discharge channel in the negative half cycle.

electron-impact dissociation, the ionization process and electron dissociative attachment [26]. And the form and rate of CO_2 molecular excitation depend on the electron temperature. Therefore, CO_2 conversion is closely related to electron density and electron temperature in plasma domain. It can be seen that the electron density reaches the maximum in the negative glow region, due to the most intense electron collision reactions in the cathode region. Then massive electrons could be generated and continue to collide with the gas molecules in the axial channel as well as the radial direction, therefore, a main plasma channel and a surrounding diffuse plasma region could be both observed in the positive column, which is in good agreement with the results in Fig. 3(b). The splitting of CO_2 is mainly caused by electron collision reaction [14], illustrating that the electron number between electrodes is positively correlated with CO_2 conversion. Fig. 4(c) shows the total electron number by integrating the electron density in the positive half circle (in Fig. 4(a)) and negative half circle (in Fig. 4(b)). It can be noted that the total electron number in the 6 mm gap demonstrates a maximum because of the sufficient distance for collision reaction and current value, indicating that the total amount of CO_2 splitting is the largest, which provides quantitative evidences for the maximum conversion and energy efficiency. Therefore, the cooperative effect of gap distance and discharge current maximizes electron number which determines CO_2 splitting.

3.3. The influence of discharge power

Fig. 5(a) shows CO_2 conversion and energy efficiency as a function of discharge power, in which the gap distance is 6 mm and the gas flow rate is 250 mL/min. It can be seen that the conversion rises with increasing discharge power, while the energy efficiency exhibits the opposite trend. The increase of discharge power means more active species in the reactor leading to higher conversion. On the other hand, larger discharge power causes more Joule heat generating and transferring to gas molecules, but higher gas temperature would accelerate the recombination of CO and O_2 and vibration translation relaxation [9], which leads to lower energy efficiency. Because of the obvious change of slope, the curve of conversion and energy efficiency with discharge power is divided into two stages. It can be found that the way to optimize the current experimental results is to continue to increase the discharge power because the conversion can be greatly improved while sacrificing a little energy efficiency in stage 2. The variation in the slope of conversion and energy efficiency may be attributed to the transition of discharge mode. Fig. 5(b) shows the images of CO_2 glow discharge morphology at different discharge powers. The exposure time of these photographs is 1/1600 s. The dash red line represents the contour of pin and plate electrodes. Through the images of CO_2 glow discharge morphology, it is obvious that there is a transition of discharge mode occurring at the discharge power of 18.35 W. When the discharge power is 7.46, 9.67 and 15.24 W, the diameters of the main discharge channel are measured to be about 0.2, 0.3 and 0.5 mm, respectively. When the power increases to 18.35 W, the diameter of the main discharge channel is 0.5 mm and remains the same even if the discharge power continues to increase, but the diffuse plasma surrounding the main channel starts to appear and grows larger along with the discharge power. Since the slope of conversion increase is larger and the slope of energy efficiency decrease is smaller in stage 2, it can be inferred that the diffuse plasma region plays a more important role in CO_2 splitting than the main discharge channel. Because the diffuse plasma region could improve the probability of CO_2 molecules passing through plasma region greatly, rapid enhancement of conversion occurs in stage 2.

Fig. 5(c) shows the simulation results of electron density distribution along discharge channel in the negative half cycle. It is found that the amplitude of electron number density rises by the increase of discharge power, indicating that higher discharge power contributes to more energetic electrons to improve the volume of plasma region. In addition, it is worthy to note that there are more electrons gathering near the anode when the discharge power is 15.70 W. This occurs because there is a streamer discharge before the glow discharge and the head of the electron avalanche reaches the anode after streamer forming. The transition of discharge form affects not only the density distribution but also the energy of active species, which could also influence splitting of CO_2. The simulation results of electron temperature distribution along the main discharge channel in the negative half circle is shown in Fig. 5(d). It should be noted that when the discharge power is 15.70 W, the electron temperature in the positive column region is lower (<2 eV). Therefore, it is difficult for electrons to participate in collision ionization along the radial electric field direction due to the low temperature of electrons, which explain that there is no diffuse plasma region around the main discharge channel when the discharge power is lower than 18 W. The reason for the drop in electron temperature could be attributed to that streamer discharge changes the distribution of space charge and causes lower reduction electric field [27]. The influence of streamer discharge divides the change curve of CO_2 conversion and energy efficiency in Fig. 5(a) into two stages. Furthermore, the electron temperature amplitude in the cathode region where electron collision reaction is most intense rises with the increase of discharge power, indicating that higher discharge power can effectively improve the probability of CO_2 collision dissociation and obtain more active particles. Hence, discharge power could modulate plasma density and electron temperature to change the active plasma volume which determines the splitting of CO_2, and the existence of streamer discharge have a significant influence on CO_2 splitting in the above process.

3.4. The influence of gas flow rate

Fig. 6(a) shows CO_2 conversion and energy efficiency as a function of gas flow rate, in which the distance between the pin-ring electrodes is set to 6 mm and the discharge power is maintained as 23 W. Generally, the conversion increases as the gas flow rate decreases from 500 mL/min to 350 mL/min, but becomes independent of the gas flow rate while the gas flow rate is below 350 mL/min. It is generally believed that the gas flow rate affects CO_2 splitting by changing the residence time [10,19]. Fig. 6 (b) shows the two-dimensional simulation results of the gas velocity distribution in the reactor. The simulation model adopts the physical field of laminar, where the gas flow rate mainly affects the flow velocity. In order to more quantitatively reflect the change of gas velocity distribution under different gas flow rates, the gas velocity at the distance of 6 mm from the ring electrode to the pin tip (brown dotted line in Fig. 7(b)) is extracted to calculate mean gas velocity, which is shown in Fig. S3. According to the distribution of gas velocity, simulation results of residence time are obtained as shown in Fig. 6(c). It can be seen that the CO_2 residence time inside the plasma region decreases from 0.0167 s to 0.0091 s when the gas flow rate becomes twice as the original value, accordingly, the conversion has dropped by approximately 30%. When the residence time is less than 0.0125 s, CO_2 conversion decreases rapidly, indicating residence time has a significant influence on the splitting of CO_2. However, when the gas flow rate is below 350 mL/min, the conversion does not continue to increase, but tends to be constant. The phenomenon arises because a portion of CO_2 is unable to participate in sufficient collision-splitting reaction in the reactor due to the non-diffusivity of APGD plasma. On the other hand, the energy efficiency exhibits an opposite tend and the maximal energy efficiency of 41.51% is achieved at 500 mL/min, because the absolute amount of CO_2 transformed is larger.

In addition, the gas velocity is higher with the larger gas flow rate, leading to the lower gas temperature which could contribute to higher energy efficiency. Fig. S4 shows the distribution of mean gas temperature at different gas flow rates. And the average gas temperatures at different gas flow rates are calculated as shown in Fig. 6(c). When the gas flow rate is 250, 300, 350, 400, 450 and 500 mL/min, the average gas temperature is 830.38, 814.50, 795.72, 777.39, 762.60 and 740.88 K respectively, indicating that gas flow could effectively reduce

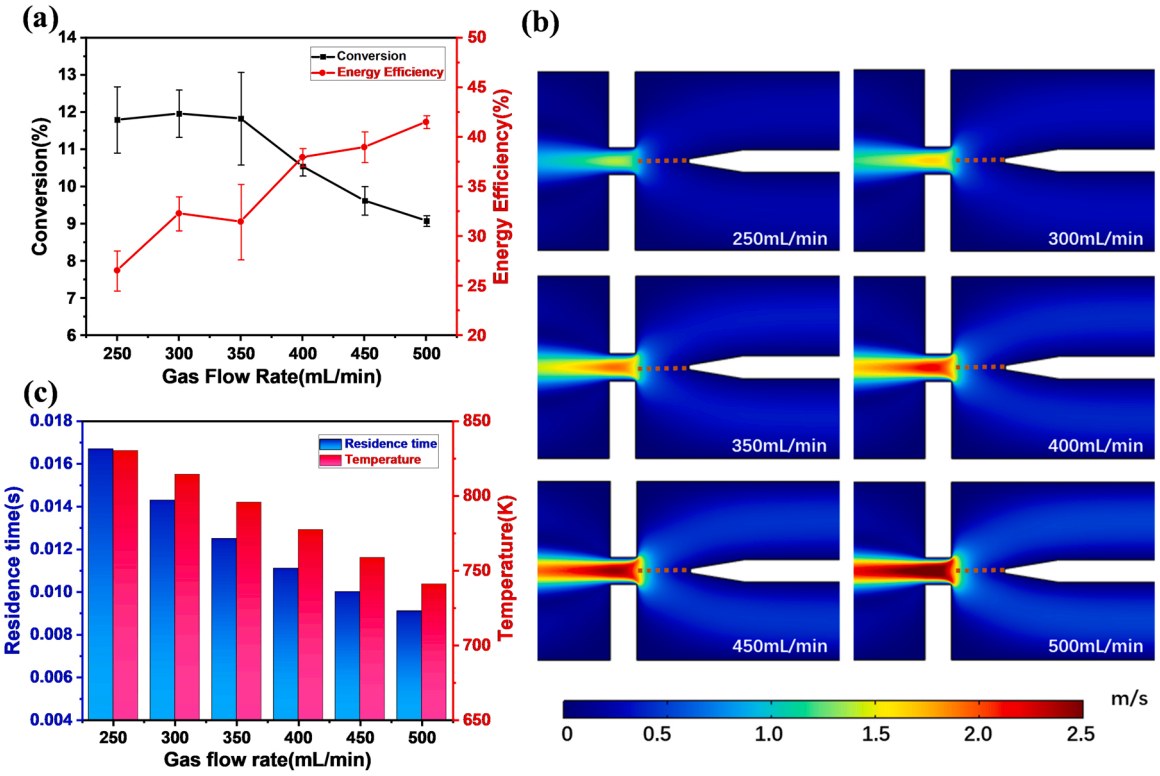

Fig. 6. (a) CO_2 conversion and energy efficiency as a function of gas flow rate, (b) the two-dimensional simulation results of the gas velocity distribution in the reactor, (c) simulation results of residence time and average gas temperature at different gas flow rates.

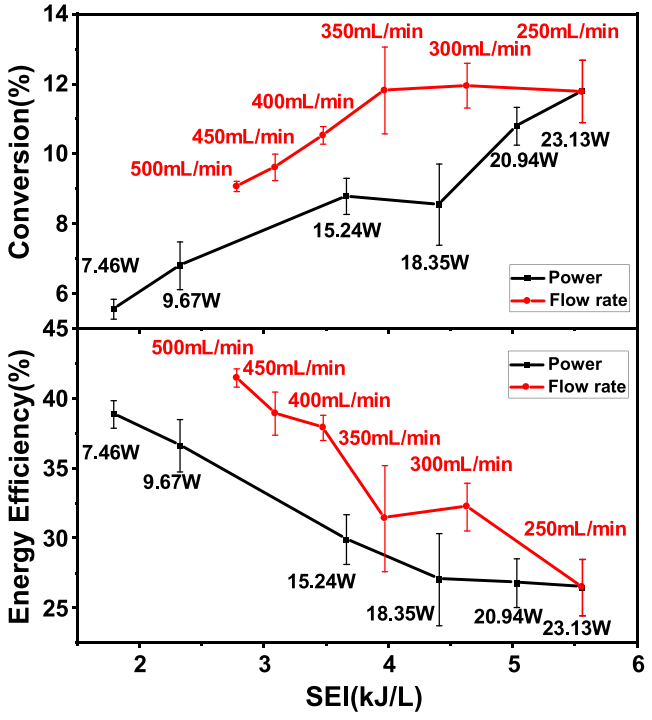

Fig. 7. CO_2 conversion and energy efficiency as a function of SEI.

the gas temperature in the APGD reactor. The recombination reaction of CO and O_2 is affected by gas temperature, and its reaction rate is positively correlated with gas temperature [28]. However, the reaction rate of CO_2 pyrolysis at high temperature is also positively correlated with temperature [13]. Table 2 shows the recombination reaction and the pyrolysis reaction.

Table 2
The recombination reaction and the pyrolysis reaction.

Reaction	Rate coefficient
$O_2 + CO \Rightarrow CO_2 + O$	$1.28 \times 10^{-18}\exp(-12{,}800/T_g)$
$CO_2 + M \Rightarrow CO + O + M$	$4.39 \times 10^{-13}\exp(-65{,}000/T_g)$

Note: M represents any neutral species taken into account in the model.

In this range of gas temperature, the reaction rate of the recombination reaction is much larger than that of the CO_2 pyrolysis reaction, indicating that the CO_2 molecules produced by the recombination reaction are far more than those transformed by pyrolysis reaction when the temperature rises. In summary, high temperature is unfavorable to CO_2 splitting by NTP, and high gas flow velocity can effectively reduce the gas temperature in the reactor.

3.5. Performance evaluation and comparison

Fig. 7 shows CO_2 conversion and energy efficiency as a function of SEI. SEI is determined by the gas flow rate and the discharge power together as shown in Eq. (3), which is considered as one of the crucial factors factor in the CO_2 conversion process [16]. The black line represents CO_2 conversion and energy efficiency as a function of discharge power when the gas flow rate was kept to 250 mL/min, the red line represents CO_2 conversion and energy efficiency as a function of gas flow rate when the discharge power was kept to 23 W. Obviously, the increased SEI is beneficial for the larger CO_2 splitting while disadvantageous for improved energy efficiency. Although the values of SEI are the same, the conversion and energy efficiency are higher when the discharge power and gas flow rate are greater, indicating that a certain SEI value obtained by the different combinations of gas flow rate and discharge power may result in different conversion performances. Remarkably, this result is absolutely different from that in DBD system

where CO_2 conversion and energy efficiency are higher when the discharge power and gas flow rate are lower [21]. This may occur due to that greater discharge power improve the volume of plasma region, leading to higher probability of collision ionization of CO_2 molecules. Besides, the high-speed flow would take away the heat from APGD reactor to prevent excessive temperature which is not beneficial for CO_2 conversion. If only either discharge power or gas flow rate is increased solely, the high conversion and energy efficiency are often incompatible. Hence, CO_2 splitting could be carried out at higher power and gas flow rate, in order to obtain the co-improved conversion and energy efficiency.

Fig. 8(a) shows the change trends of the densities of vibrational and excited states. In APGD, the vibrational and excited state with the maximum density is CO_2va, the following are CO_2vb, CO_2vc, CO_2vd and CO_2s, because the vibration and excited states at higher energy level have smaller density. It could be considered that vibrational excitation plays a vital role in the process of CO_2 molecular excitation for APGD leading to considerable energy efficiency. Besides, the number density of vibrational and excited states rises faster at the beginning of reaction, which may be attributed to the higher density of ground state CO_2. Fig. 8 (b) shows the change trends of the densities of CO, O, O_2 and CO_2. The density of CO_2 decreases rapidly at the beginning of reaction due to the fast vibrational excitation of CO_2 molecule, which is consistent with Fig. 8(a). It could be found that the density of CO, O and O_2 increases in a stepwise trend over time. This may occur due to that the recombination rate between products is greater than or equal to the CO_2 dissociation rate when discharge current is lower. The number density of three neutral particles presents this law: $n(CO)>n(O)>n(O_2)$, which is consistent with the phenomenon described in Ref. [29,30]. According to Fig. 8(a) and (b), it is concluded that the energy of electrons is first transferred to the vibrational state, and the ground state CO_2 is dissociated by step-by-step vibration excitation by electron impact. Although the recombination rate is higher than or equal to the dissociation rate at certain moments, the particle density of the product shows an overall upward trend.

Fig. 9 shows the energy efficiency and conversion for pure CO_2 dissociation using different reactor configurations reported in previous literatures. Although larger CO_2 conversion and energy efficiency could be achieved using MW and RF plasma for CO_2 splitting [11,12,31,32], these only could be obtained at low pressure environment. Besides, the plasma systems of MW and RF are complex and expensive which are unfavorable for industrial application. DBD [7,21,33–36] have good performance in terms of CO_2 conversion (15–30%) due to excellent diffusivity of plasma. However, with higher reduction electric field (>100 Td), the form of CO_2 excitation is mainly direct excitation rather than vibration excitation in DBD leading to that their energy efficiency has been limited to less than 10%. With lower reduction electric field, GA provides high energy efficiency, but has poor performance in

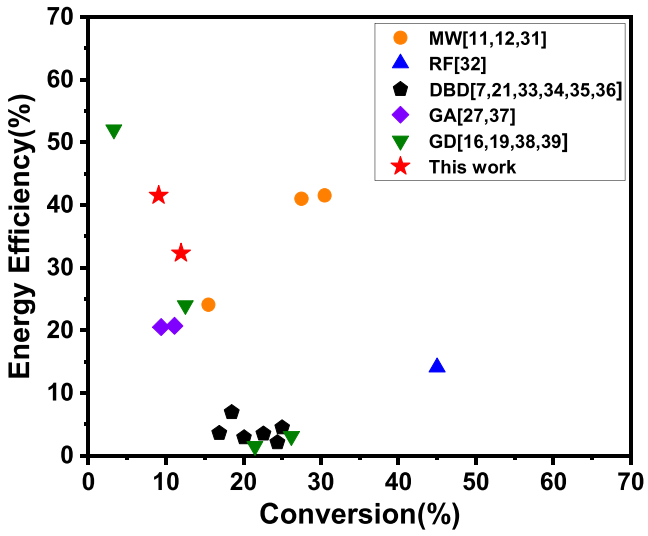

Fig. 9. Energy efficiency versus conversion for pure CO_2 splitting using various reactor configurations. (DBD: dielectric barrier discharge, MW: microwave, RF: radio frequency, GD: glow discharge, GA: gliding arc).

conversion due to the non-diffuse plasma area [27,37]. CO_2 splitting by glow discharge (GD) has two different characteristics. The conversion is higher since the large plasma volume at low pressure, but the amount of CO_2 processed per unit time is limited, resulting in absolutely low energy efficiency [38,39]. The realization of APGD makes GD have more applications in CO_2 splitting, which is manifested in considerable energy efficiency but lower conversion [16,19]. In our work, we proposed the AC-driven APGD reactor for CO_2 splitting, and conducted a comprehensive study on the influence mechanism of CO_2 splitting. The influence of gap distance in APGD on CO_2 splitting is discovered for the first time, selecting an appropriate gap distance could optimize the plasma reactor to co-improve the conversion and energy efficiency synergistically. By comparing the influences of different factors systematically, we further uncovered that the conversion and energy efficiency could be co-improved by synchronously increasing the discharge power and gas flow rate at a given SEI value, which exhibits an opposite feature of DBD plasma. Finally, the best performance with CO_2 conversion of 9.08% and energy efficiency of 41.51% is obtained due to the above synergistic effects, performing better than those of most DBD, GA and GD.

4. Conclusion

In this work, we have realized stable APGD driven by AC using pin-plate electrodes and investigated the influences of gap distance, discharge power, gas flow rate on CO_2 splitting by experiments and

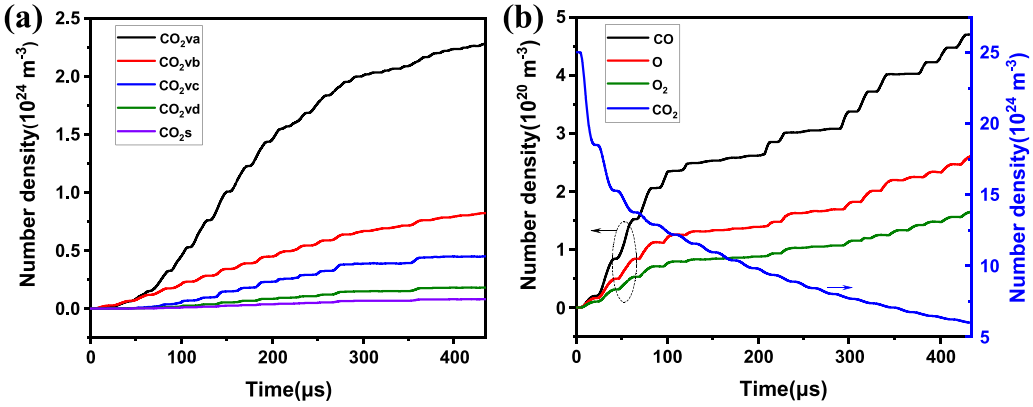

Fig. 8. The change trends of neutral particles density with time: (a) density variation of vibrational and excited states, (b) density variation of CO, O, O_2 and CO_2.

simulations. The results show that adjusting gap distance for APGD reactor could achieve co-improved conversion and energy efficiency, because sufficient electron collisions along the main channel result in the largest active plasma volume at an appropriate gap distance. The results of FEM simulation reveal that the distributions of electron density and temperature determine the active plasma volume which is a crucial factor for CO_2 splitting. The emergence of streamer discharge at lower discharge power decreases the electron temperature and dissipate the diffuse plasma region, which eventually reduces the overall active plasma volume for CO_2 splitting. CO_2 conversion remains nearly constant when gas flow rate is below 350 mL/min due to the non-diffusivity, and declines rapidly when gas flow rate is above 350 mL/min on account of the residence time reduction. Energy efficiency is positively correlated with gas flow rate, due to the increase of the absolute CO_2 transformed amount and the decrease of gas temperature at higher gas flow rate. At a certain SEI value, the conversion and energy efficiency can be co-improved when the discharge power and gas flow rate are greater due to the larger active plasma volume and lower gas temperature. We have achieved a maximum conversion of 11.96% and maximum energy efficiency of 41.51% which are better than the results of most DBD and GA.

This work is a preliminary study for the further combination with catalysts. Based on the interesting results and the regulation of the APGD plasma, future work will focus on the realization of synergy between catalyst and APGD. The optimization of reactor and catalyst will also be investigated to obtain better synergistic effect on CO_2 conversion, which will pave the way to possible industrial application.

CRediT authorship contribution statement

Guodong Meng: Conceptualization, Methodology, Investigation, Writing – original draft, Writing – review & editing, Funding acquisition. **Linghan Xia:** Methodology, Software, Formal analysis, Investigation, Writing – original draft. **Yonghong Cheng:** Resources, Supervision, Project administration. **Zongyou Yin:** Conceptualization, Methodology, Investigation, Writing – review & editing, Visualization.

Declaration of Competing Interest

The authors declare that they have no known competing financial interests or personal relationships that could have appeared to influence the work reported in this paper.

Data availability

Data will be made available on request.

Acknowledgments

This work was partially supported by State Key Laboratory of Electrical Insulation and Power Equipment (EIPE22315) and the National Natural Science Foundation of China (51977169).

Appendix A. Supplementary material

Supplementary data associated with this article can be found in the online version at doi:10.1016/j.jcou.2023.102447.

References

[1] L. Wang, W. Chen, D. Zhang, Y. Du, R. Amal, S. Qiao, J. Wu, Z. Yin, Surface strategies for catalytic CO_2 reduction: from two-dimensional materials to nanoclusters to single atoms, Chem. Soc. Rev. 48 (2019) 5310–5349, https://doi.org/10.1039/C9CS00163H.

[2] Rosa M. Cuéllar-Franca, Adisa Azapagic, Carbon capture, storage and utilisation technologies: a critical analysis and comparison of their life cycle environmental impacts, J. CO_2 Util. 9 (2015) 82–102, https://doi.org/10.1016/j.jcou.2014.12.001.

[3] R. Snoeckx, A. Bogaerts, Plasma technology – a novel solution for CO_2 conversion? Chem. Soc. 46 (2017) 5805–5863, https://doi.org/10.1039/C6CS00066E.

[4] S. Xu, H. Chen, C. Hardacre, X. Fan, Non-thermal plasma catalysis for CO_2 conversion and catalyst design for the process, J. Phys. D Appl. Phys. 54 (2021), 233001, https://doi.org/10.1088/1361-6463/abe9e1.

[5] Xin Li, Haopeng Jiang, Changchang Ma, Zhi Zhu, Xianghai Song, Huiqin Wang, Pengwei Huo, Xiuyan Li, Local surface plasma resonance effect enhanced Z-scheme ZnO/Au/g-C_3N_4 film photocatalyst for reduction of CO_2 to CO, Appl. Catal. B 283 (2021), 119638, https://doi.org/10.1016/j.apcatb.2020.119638.

[6] Guoxing Chen, Violeta Georgieva, Thomas Godfroid, Rony Snyders, Marie-Paule Delplancke-Ogletree, Plasma assisted catalytic decomposition of CO_2, Appl. Catal. B 190 (2016) 115–124, https://doi.org/10.1016/j.apcatb.2016.03.009.

[7] M. Zhu, S. Hu, F. Wu, H. Ma, S. Xie, C. Zhang, CO_2 dissociation in a packed bed DBD reactor: effect of streamer discharge, J. Phys. D Appl. Phys. 55 (2022), 225207, https://doi.org/10.1088/1361-6463/ac55c1.

[8] Bryony Ashford, Yaolin Wang, Chee-Kok Poh, Luwei Chen, Xin Tu, Plasma-catalytic conversion of CO_2 to CO over binary metal oxide catalysts at low temperatures, Appl. Catal. B 276 (2020), 119110, https://doi.org/10.1016/j.apcatb.2020.119110.

[9] A. Bogaerts, G. Centi, Plasma technology for CO_2 conversion: a personal perspective on prospects and gaps front, Energy Res. 8 (2020) 111, https://doi.org/10.3389/fenrg.2020.00111.

[10] L. Li, H. Zhang, X. Li, J. Huang, X. Kong, R. Xu, X. Tu, Magnetically enhanced gliding arc discharge for CO_2 activation, J. CO_2 Util. 35 (2020) 28–37, https://doi.org/10.1016/j.jcou.2019.08.021.

[11] W. Bongers, H. Bouwmeester, B. Wolf, F. Peeters, S. Welzel, D. van den Bekerom, N. den Harder, A. Goede, M. Graswinckel, P.W. Groen, J. Kopecki, M. Leins, G. van Rooij, A. Schulz, M. Walker, R. van de Sanden, Plasma-driven dissociation of CO_2 for fuel synthesis, Plasma Process Polym. 14 (2017), 1600126, https://doi.org/10.1002/ppap.201600126.

[12] G.J. Van Rooij, D.C.M. van den Bekerom, N. den Harder, T. Minea, G. Berden, W. A. Bongers, R. Engeln, M.F. Graswinckel, E. Zoethout, M.C.M. van de Sanden, Taming microwave plasma to beat thermodynamics in CO_2 dissociation, Faraday Discuss. 183 (2015) 233–248, https://doi.org/10.1039/C5FD00045A.

[13] A. Berthelot, A. Bogaerts, Modeling of CO_2 splitting in a microwave plasma: how to improve the conversion and energy efficiency, J. Phys. Chem. C 121 (2017) 8236–8251, https://doi.org/10.1021/acs.jpcc.6b12840.

[14] G. Trenchev, S. Kolev, A. Bogaerts, A 3D model of a reverse vortex flow gliding arc reactor, Plasma Sources Sci. Technol. 25 (2016), 035014, https://doi.org/10.1088/0963-0252/25/3/035014.

[15] Y. Wang, W. Liu, W. Ding, Study of the characteristic differences of positive and negative half-cycles from atmospheric pressure glow discharge driven by resonant AC voltage, AIP Adv. 11 (2021), 075002, https://doi.org/10.1063/5.0046139.

[16] G. Trenchev, A. Nikiforov, W. Wang, St Kolev, A. Bogaerts, Atmospheric pressure glow discharge for CO_2 conversion: model-based exploration of the optimum reactor configuration, Chem. Eng. J. 362 (2019) 830–841, https://doi.org/10.1016/j.cej.2019.01.091.

[17] F. Tochikubo, A. Komuro, Review of numerical simulation of atmospheric-pressure non-equilibrium plasmas: streamer discharges and glow discharges, Jpn. J. Appl. Phys. 60 (2021), 040501, https://doi.org/10.35848/1347-4065/abe6e2.

[18] J. Chao, W. Youqing, Formation of large-volume high-pressure plasma in triode-configuration discharge devices, Plasma Sci. Technol. 8 (2006) 185–189, https://doi.org/10.1088/1009-0630/8/2/13.

[19] B. Raja, R. Sarathi, R. Vinu, Development of a swirl-induced rotating glow discharge reactor for CO_2 conversion: fluid dynamics and discharge dynamics studies, Energy Technol. 8 (2020), 2000535, https://doi.org/10.1002/ente.202000535.

[20] D. Staack, B. Farouk, A. Gutsol, A. Fridman, Characterization of a dc atmospheric pressure normal glow discharge, Plasma Sources Sci. Technol. 14 (2005) 700–711, https://doi.org/10.1088/0963-0252/14/4/009.

[21] G. Niu, Y. Qin, W. Li, Y. Duan, Investigation of CO_2 splitting process under atmospheric pressure using multi-electrode cylindrical DBD plasma reactor, Plasma Chem. Plasma Process. 39 (2019) 809–824, https://doi.org/10.1007/s11090-019-09955-y.

[22] T. Kozák, A. Bogaerts, Splitting of CO_2 by vibrational excitation in non-equilibrium plasmas: a reaction kinetics model, Plasma Sources Sci. Technol. 23 (2014), 045004, https://doi.org/10.1088/0963-0252/23/4/045004.

[23] Feng Li Weidong Ding, Lanjun Yang, Atmospheric-pressure glow discharge sustained by a resonant power supply, IEEE Trans. Plasma Sci. 37 (2009) 2207–2212, https://doi.org/10.1109/TPS.2009.2030202.

[24] S. Wu, W. Cheng, G. Huang, F. Wu, C. Liu, X. Liu, C. Zhang, X. Lu, Positive streamer corona, single filament, transient glow, dc glow, spark, and their transitions in atmospheric air, Phys. Plasmas 25 (2018), 123507, https://doi.org/10.1063/1.5042669.

[25] G. Meng, Q. Ying, A.M. Loveless, F. Wu, K. Wang, Y. Fu, A.L. Garner, Y. Cheng, Spatio-temporal dynamics of pulsed gas breakdown in microgaps, Phys. Plasmas 26 (2019), 014506, https://doi.org/10.1063/1.5081009.

[26] S. Xu, H. Chen, C. Hardacre, et al., Non-thermal plasma catalysis for CO_2 conversion and catalyst design for the process, J. Phys. D Appl. Phys. 54 (2021), 233001, https://doi.org/10.1088/1361-6463/abe9e1.

[27] L. Li, H. Zhang, X. Li, X. Kong, R. Xu, K. Tay, X. Tu, Plasma-assisted CO_2 conversion in a gliding arc discharge: improving performance by optimizing the reactor design, J. CO_2 Util. 29 (2019) 296–303, https://doi.org/10.1016/j.jcou.2018.12.019.

[28] A. Fridman, S. Nester, L.A. Kennedy, A. Saveliev, O. Mutaf-Yardimci, Gliding arc gas discharge, Prog. Energy Combust. Sci. 25 (1999) 211–231, https://doi.org/10.1016/S0360-1285(98)00021-5.

[29] R. Aerts, T. Martens, A. Bogaerts, Influence of vibrational states on CO_2 splitting by dielectric barrier discharges, J. Phys. Chem. C 116 (2012) 23257–23273, https://doi.org/10.1021/jp307525t.

[30] W. Wang, A. Berthelot, S. Kolev, X. Tu, A. Bogaerts, CO_2 conversion in a gliding arc plasma: 1D cylindrical discharge model, Plasma Sources Sci. Technol. 25 (2016), 065012, https://doi.org/10.1088/0963-0252/25/6/065012.

[31] S. Mohsenian, D. Nagassou, S. Bhatta, R. Elahi, J.P. Trelles, Design and characterization of a solar-enhanced microwave plasma reactor for atmospheric pressure carbon dioxide decomposition, Plasma Sources Sci. Technol. 28 (2019), 065001, https://doi.org/10.1088/1361-6595/ab1c43.

[32] E.J. Devid, M. Ronda-Lloret, D. Zhang, E. Schuler, D. Wang, C.-H. Liang, Q. Huang, G. Rothenberg, N.R. Shiju, A.W. Kleyn, Enhancing CO_2 plasma conversion using metal grid catalysts, J. Appl. Phys. 129 (2021), 053306, https://doi.org/10.1063/5.0033212.

[33] W. Ding, M. Xia, C. Shen, Y. Wang, Z. Zhang, X. Tu, C. Liu, Enhanced CO_2 conversion by frosted dielectric surface with ZrO_2 coating in a dielectric barrier discharge reactor, J. CO_2 Util. 61 (2022), 102045, https://doi.org/10.1016/j.jcou.2022.102045.

[34] B. Wang, X. Wang, H. Su, Influence of electrode interval and barrier thickness in the segmented electrode micro-plasma DBD reactor on CO_2 decomposition, Plasma Chem. Plasma Process. 40 (2020) 1189–1206, https://doi.org/10.1007/s11090-020-10091-1.

[35] I. Michielsen, Y. Uytdenhouwen, J. Pype, B. Michielsen, J. Mertens, F. Reniers, V. Meynen, A. Bogaerts, CO_2 dissociation in a packed bed DBD reactor: first steps towards a better understanding of plasma catalysis, Chem. Eng. J. 326 (2017) 477–488, https://doi.org/10.1016/j.cej.2017.05.177.

[36] D. Mei, X. Tu, Atmospheric pressure Non-thermal plasma activation of CO_2 in a packed-bed dielectric barrier discharge reactor, ChemPhysChem 18 (2017) 3253–3259, https://doi.org/10.1002/cphc.201700752.

[37] H. Sun, Z. Chen, J. Chen, H. Long, Y. Wu, W. Zhou, The influence of back-breakdown on the CO_2 conversion in gliding arc plasma: based on experiments of different materials and improved structures, J. Phys. D Appl. Phys. 54 (2021), 495203, https://doi.org/10.1088/1361-6463/ac2335.

[38] T. Ma, H.-X. Wang, Q. Shi, S.-N. Li, S.-R. Sun, A.B. Murphy, Experimental study of CO_2 decomposition in a DC micro-slit sustained glow discharge reactor, Plasma Chem. Plasma Process. 39 (2019) 825–844, https://doi.org/10.1007/s11090-019-09996-3.

[39] S.L. Brock, M. Marquez, S.L. Suib, Y. Hayashi, H. Matsumoto, Plasma decomposition of CO_2 in the presence of metal catalysts, J. Catal. 180 (1998) 225–233, https://doi.org/10.1006/jcat.1998.2258.